

Self-organization and transition to turbulence in randomly forced isotropic fluid motion

W. D. McComb,¹ M. F. Linkmann,¹ A. Berera,¹ S. R. Yoffe,² and B. Jankauskas¹

¹*SUPA, School of Physics and Astronomy, University of Edinburgh, UK*

²*SUPA, Department of Physics, University of Strathclyde, Glasgow, UK*

We observe a symmetry-breaking transition to a self-organized state in direct numerical simulation of the Navier-Stokes equation with random, isotropic forcing at very low Reynolds number. In this state the kinetic energy is contained only in modes at the lowest resolved wavenumber, the skewness vanishes, and visualization of the flows shows a lack of small-scale structure, with the vorticity and velocity vectors becoming aligned (a Beltrami flow). We infer from this the existence of a lower critical Reynolds number for transition to isotropic turbulence.

PACS numbers: 05.65.+b, 47.20.Ky, 47.27.Cn

One of the better known results in the history of science is the discovery of the laminar-turbulence transition in pipe flow by Osborne Reynolds in the late nineteenth century. Since then such transitions have been found in many other flow configurations, and the subject is widely studied today. In contrast, the commonly accepted view of randomly forced isotropic fluid motion is that the motion is turbulent for all Reynolds numbers and no actual transition to turbulence occurs.

In the course of studying the direct numerical simulation (DNS) of forced isotropic turbulence, we have found that self-organized states form at low Taylor-Reynolds numbers. We observed depletion of the nonlinear term in the Navier-Stokes equation (NSE) during the formation of the self-organized state. Visualization of the flow showed that the velocity field in the self-organized state is a Beltrami field [1], where velocity \mathbf{u} and vorticity $\boldsymbol{\omega} = \nabla \times \mathbf{u}$ are aligned in real space, forcing the nonlinear term $\mathbf{u} \times \boldsymbol{\omega}$ in the NSE to vanish. As this is a condition for maximum helicity, and the initial state has zero helicity, it follows that the transition to the self-ordered state is symmetry-breaking. Moreover, the flow shows only large-scale structure, consistent with the measured unimodal ($k = 1$) energy spectra, where $k = 2\pi/L_{box} = 1$ is the smallest resolved wavenumber in the simulations.

We note that our simulation method is both conventional and widely used, so we give only some necessary details here. The incompressible forced NSE was solved numerically, using the standard pseudospectral method on a 3D periodic domain of length $L_{box} = 2\pi$. Full dealiasing was achieved by truncation according to the two-thirds rule, and the system was forced by negative damping, with the Fourier transform of the force \mathbf{f} given by

$$\begin{aligned} \mathbf{f}(\mathbf{k}, t) &= (\varepsilon_W/2E_f)\mathbf{u}(\mathbf{k}, t) \quad \text{for } 0 < |\mathbf{k}| < k_f; \\ &= 0 \quad \text{otherwise,} \end{aligned} \quad (1)$$

where $\mathbf{u}(\mathbf{k}, t)$ is the instantaneous velocity field (in wavenumber space). The highest forced wavenumber, k_f , was chosen to be $k_f = 2.5k_{min}$, where $k_{min} = 2\pi/L_{box} = 1$ is the lowest resolved wavenumber. As E_f was the total energy contained in the forcing band, this ensured that

the energy injection rate was $\varepsilon_W = \text{constant}$. The initial conditions were random (Gaussian) velocity fields with prescribed energy spectra of the form

$$E(k) = C_1 k^4 e^{-C_2 k^2}, \quad (2)$$

where $C_1 = 0.001702$ and $C_2 = 0.08$. Full details of our numerical technique and code validation may be found in [2]. The initial kinetic helicity $\langle \mathbf{u}(\mathbf{k})\boldsymbol{\omega}(-\mathbf{k}) \rangle$, where $\boldsymbol{\omega}(\mathbf{k})$ is the Fourier transform of the vorticity field $\boldsymbol{\omega}(\mathbf{x})$, was negligible for all simulations. All simulations were well resolved, satisfying $k_{max}\eta \geq 2.16$ [3], where η denotes the Kolmogorov dissipation scale. The maximum time the simulations were evolved for was $t = 1000s$, or, in terms of initial large-eddy turnover times $t_0 = U/L$, $t = 1270.82t_0$. Initial Taylor-Reynolds numbers R_λ ranged from $R_\lambda = 2.61$ to $R_\lambda = 3.78$. A summary of simulation details is given in [4].

We found that a choice of 32^3 collocation points proved to be sufficient in order to resolve the Kolmogorov dissipation scale, as all our simulations were at very low Reynolds numbers. We did however verify that the formation of the self-organized state was also observed at a higher resolution (64^3).

The onset of a self-organised state is illustrated in Fig. 1 for the run where the initial Taylor-Reynolds number was $R_\lambda = 3.39$. In general we found that, after long running times, the total energy ceased to fluctuate, and instead remained constant, while the skewness dropped to zero. Once this happened, the kinetic energy was confined to the $k = 1$ mode and the nonlinear transfer had become zero, which can be seen in Fig. 2. The cascade process was thus absent and no small-scale structures were being formed. Hence the system had self-organized into a large-scale state.

The formation of this self-organized state has been observed, using both our own code and the publicly available code `hit3d` [5, 6] as shown in Fig. 1(a). Figure 1(b) shows the evolution of the velocity derivative skewness. Note that it drops to zero at long times, indicating that the observed state is Gaussian and hence is not turbulent. As the velocity derivative skewness is not recorded by `hit3d`, a comparison using this quantity was not pos-

sible.

The development of this state was accompanied by a depletion of nonlinearity, as shown in Fig. 2(a), where the transfer spectrum $T(k)$ is plotted at different times. It is clear from the figure that $T(k)$ at early times has the behaviour typically found in simulations of isotropic turbulence (see *e. g.* Fig. 5.3f, p. 126 of [2] and Fig. 9.3, p. 293 of [7]), but at later times tends to zero. At the same time, the energy spectrum $E(k)$, shown in Fig. 2(b), tends to a unimodal spectrum at $k = 1$.

Since the energy spectrum in the self-organized state is unimodal at $k = 1$, we can predict the asymptotic value $E(t) = E_\infty$ in this state from the energy input rate ε_W and the viscosity ν , by invoking stationarity ($\varepsilon_W = \varepsilon$, where ε denotes the dissipation rate), and obtain for the total energy after self-organization as

$$E(t) = E_\infty = \frac{\varepsilon_W}{2\nu} = \text{constant} . \quad (3)$$

All runs for all values of the initial Taylor-Reynolds number stabilized at this value of $E(t)$. Note that the same value is obtained both with our code and with `hit3d` as shown in Fig. 1(a).

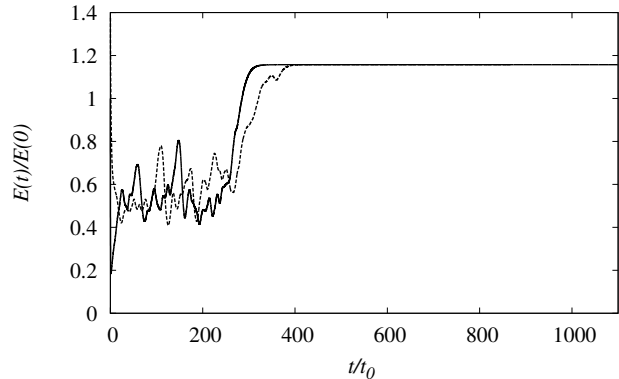
The self-organized state has a further interesting property: it is a large-scale Beltrami field. From the visualizations we may see that the vorticity field $\boldsymbol{\omega}(\mathbf{x})$ and the velocity field $\mathbf{u}(\mathbf{x})$ align with each other once the system has self-organized, such that

$$\nabla \times \mathbf{u}(\mathbf{x}) = \boldsymbol{\omega}(\mathbf{x}) = \alpha \mathbf{u}(\mathbf{x}) , \quad (4)$$

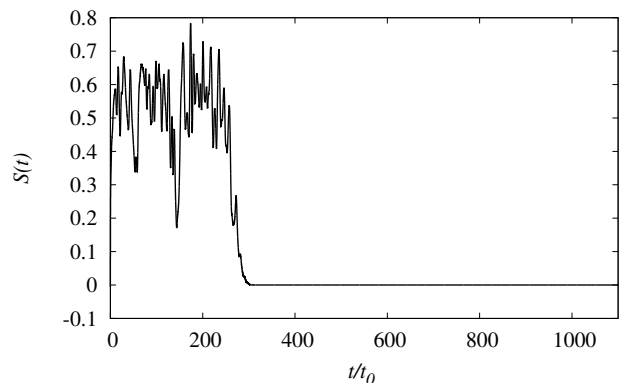
for a coefficient α (which must have dimensions of inverse length). Vector fields satisfying (4) are eigenfunctions of the curl operator and therefore helical. It should be noted that the nonlinear term in the NSE vanishes identically if the velocity and vorticity fields are aligned. Fig. 3 shows snapshots of the system before and after self-organization. The arrows indicate the velocity and vorticity fields at different points in real space. From the image on the right hand side of the figure, it can clearly be seen that the flow is in an ordered state, as velocity and vorticity vectors are everywhere parallel to each other, giving visual evidence of the Beltrami property (4) of the large-scale field. Furthermore, we observe a lack of small-scale structure of the flow, which reflects the measured unimodal energy spectrum in the self-organized state. The Beltrami condition has also been verified by analyzing helicity spectra, showing nonzero helicity at $k = 1$ and zero helicity at all higher wavenumbers.

A short film showing the transition to the self-organized state can be found in [4]. Two interesting points may be observed from the film. First, the system shows behaviour similar to ‘critical slowing down’. Secondly, we observe a transition from a non-helical state to a helical state. That is, the formation of the helical self-organized state is symmetry-breaking. This latter aspect can also be seen in Fig. 3.

The formation of the self-organized state was found to occur at progressively later times as we increased the



(a) Evolution of the total energy



(b) Evolution of the skewness

FIG. 1. Onset of the self-organized state as indicated by the total energy $E(t)$ and the velocity-derivative skewness $S(t)$ for $R_\lambda = 3.39$. (a) $E(t)$: the solid line shows results from our DNS and the dashed line results from `hit3d`. Note that both codes produce a self-organized state at the same value of the total energy, as predicted by (3). (b) $S(t)$: evolution of the skewness for the same run. Note that the skewness falls to zero at much the same time as the occurrence of the plateau at $E(t) = E_\infty$ in (a).

Reynolds number. Similar observations have been made in studies of the transition to turbulence in shear flows in connection with the sudden breakdown of localized turbulence. Drawing an analogy with relaminarization of a turbulent puff must be done with some caution, as randomly stirred fluid motion and pressure driven pipe flow are very different systems. Nevertheless, we may hope to obtain some guidance from a consideration of the rather similar problem of the Reynolds-number dependence of the characteristic time scale in pipe flows [8–11].

In order to study the Reynolds number dependence of the characteristic time τ^* at which the self-organized state formed, we populated ensembles with 100 runs for

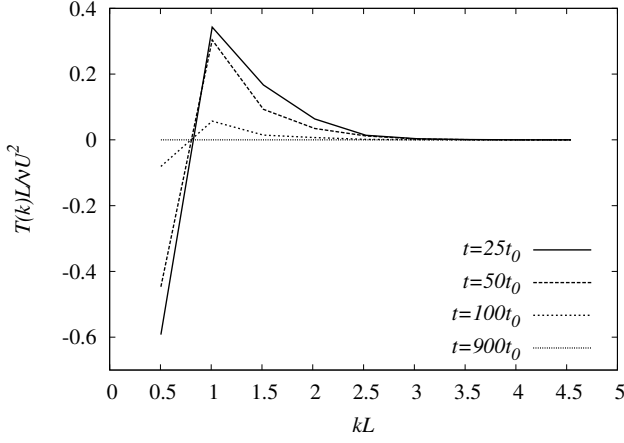
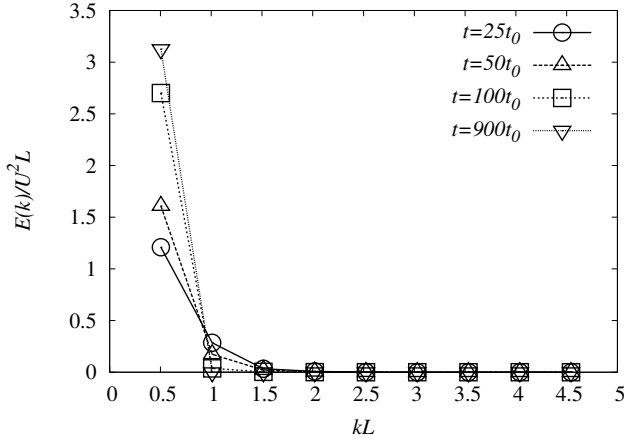
(a) Transfer spectra at different times for $R_\lambda = 3.39$.(b) Energy spectra at different times for $R_\lambda = 3.39$.

FIG. 2. (a) Transfer spectra at different times showing the depletion of nonlinearity as the nonlinear transfer gets weaker as time progresses. The time evolution of the total energy corresponding to the measured spectra is shown in Fig. 1(a). (b) Energy spectra at different times. The formation of a unimodal spectrum is clearly visible. After self-organization only the $k = 1$ mode remains populated while all other modes have lost their kinetic energy. The kinetic energy is therefore concentrated in the large scales and we do not expect small-scale flow patterns. This corresponds to the right-hand image of Fig. 3, where the flow shows only large-scale structure.

each initial Reynolds number. The relevant spectral quantities of each sampled velocity field were first shell-averaged. Then we calculated the total energy $E(t)$, the dissipation rate $\varepsilon(t)$ and the skewness $S(t)$, for each simulation belonging to a given ensemble. We considered three different criteria for the determination of the self-organization time τ of a single simulation, that is: (a) the time at which the specific value of $E(t) = E_\infty$ as in Eq. (3) was reached; (b) the time at which the dissipation rate equalled the input rate without any fluctuations; and (c) the time at which the skewness had dropped to zero.

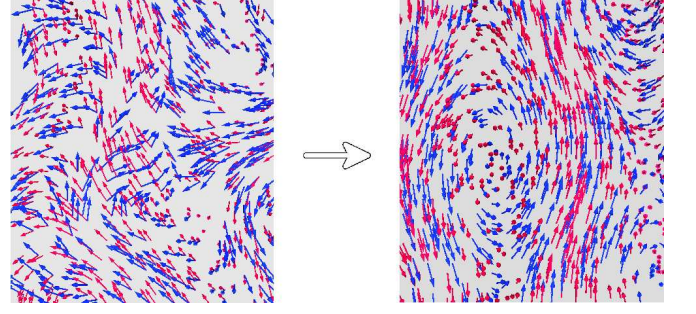


FIG. 3. (Color online) Visualization of the velocity field (red arrows) and the vorticity field (blue arrows) in x -space before and after self-organization. The alignment between velocity and vorticity fields is clearly visible in the right-hand image.

As all three gave much the same results, we used (c) for convenience.

For a preliminary analysis, we took the ensemble average $\tau^* = \langle \tau \rangle$ for each initial Taylor-Reynolds number. We then tested the effect of two fitting different functional forms to the data. That is, an exponential: $\tau^* = \exp[A + BR_\lambda]$, and also a power law of the form $\tau^* = C/(R_{\lambda,crit} - R_\lambda)^\alpha$, where A, B, C and α are constants. It turned out that the power law produced the better fit. This was interpreted as demonstrating critical behaviour and was found to lead to a critical Reynolds number of $R_{\lambda,crit} = 4.16$.

We also found that although some single realizations showed temporary stationary-state behavior (that is, the total energy $E(t)$ fluctuated about a mean value), other realizations did not show such behavior. Moreover, the ensemble average of $E(t)$ (and thus, by definition, the system) did *not* reach such an intermediate stationary state. Had the ensemble average reached a stationary state, then its profile of $E(t)$ would have shown a plateau at the mean value and later a sharp increase towards the self-organized state value of the total energy E_∞ . Instead, as can be seen in Fig. 4, the total energy of the ensemble average increases nearly monotonically until the self-organized state value given by (3) is reached. For all the ensembles which we examined, the same basic features were seen as in Fig. 4, where the ensemble average is plotted alongside four individual realizations, two of which show stationary-state behavior and two which do not. The common feature of all realizations is the formation, ultimately, of the self-organized state. This result may have implications for the assumption of ergodic behavior of the dynamical system at low Reynolds numbers.

It is possible to put forward (at least) two phenomenological arguments for the existence of an upper critical Reynolds number for the formation of large-scale helical states. First, as suggested by the measurements of τ^* , the formation of a self-organized state becomes less likely with increasing Reynolds number. This in itself seems to

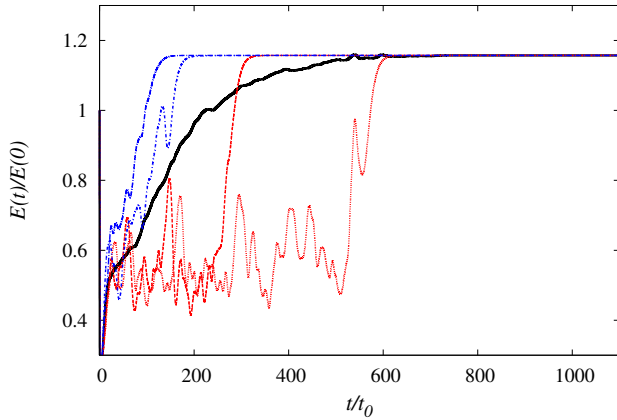


FIG. 4. (Color online) Comparison of the ensemble average (thick solid line) with four realizations (dashed, dotted and dash-dotted lines) of the flow for an ensemble at $R_\lambda = 3.72$ ($\nu = 0.07$). The ensemble average shows no fluctuations of $E(t)$ about a mean value contrary to two of the chosen four realizations (dotted and dashed lines, on the right of the solid line), which show steady-state behaviour. The other two realizations (dash-dotted lines on the left of the solid line) do not show steady-state behaviour.

indicate the presence of a Reynolds number above which the flow does not self-organize into a Beltrami state. Assuming that there is a large-scale Beltrami-component to the flow, we now ask if there is a Reynolds number threshold above which the forward cascade feeding into the small scales is sufficient to maintain a fully turbulent flow.

For this purpose we decompose the velocity field into \mathbf{u}_0 , the large-scale Beltrami component of the velocity field \mathbf{u} , and \mathbf{u}' the small(er)-scale component of \mathbf{u} , such that:

$$\mathbf{u} = \mathbf{u}_0 + \mathbf{u}' . \quad (5)$$

If the small-scale component decays away, then at long times we will observe $\mathbf{u} = \mathbf{u}_0$.

Consider the evolution equation for \mathbf{u}' (as obtained from the NSE),

$$\partial_t \mathbf{u}' = -\nabla P + \mathbf{u}' \times \boldsymbol{\omega}_0 + \mathbf{u}' \times \boldsymbol{\omega}' + \mathbf{u}_0 \times \boldsymbol{\omega}' + \nu \Delta \mathbf{u}' , \quad (6)$$

where the term $\mathbf{u}_0 \times \boldsymbol{\omega}_0 = 0$ is not present since \mathbf{u}_0 is a Beltrami field. The additional gradient terms that arise from writing the nonlinear terms as vector cross products have been absorbed into the pressure P . Note that the forcing has been omitted from (6), since the velocity field is forced at the large scales and the small-scale field only receives energy through the forward spectral space energy cascade from the large-scale field. By taking the scalar product with \mathbf{u}' on both sides of (6) and integrating over all space we obtain an evolution equation for the total

energy (per unit volume) $E'(t)$ of the small-scale field

$$\partial_t E'(t) = \int_{\mathbb{R}^3} d\mathbf{x} \, \mathbf{u}' \cdot (\mathbf{u}_0 \times \boldsymbol{\omega}') - \nu \int_{\mathbb{R}^3} d\mathbf{x} \, \boldsymbol{\omega}'^2 . \quad (7)$$

Then, whether $E'(t)$ grows or decays over time, depends on whether or not the transfer term in (7) dominates over the dissipative term. In other words, there must be a Reynolds number below which the small-scale component decays away and the Beltrami component is stable.

Although this theoretical analysis does not produce a numerical estimate of the actual Reynolds number below which a self-organized Beltrami state is stable, it shows that such a Reynolds number should exist.

A second argument against the existence of self-organized Beltrami states at high Reynolds number follows from the symmetry-breaking nature of the transition and the approximate conservation (*i. e.* inviscid conservation) of kinetic helicity at high Reynolds numbers. All initial velocity fields in our simulations are nonhelical, but the self-organized state is unimodal *and* maximally helical. The formation of a unimodal helical state is incompatible with the conservation of kinetic helicity, since no other mode is populated which could compensate for the nonzero helicity at $k = 1$, and this would be necessary as we started the simulation with zero kinetic helicity. Therefore self-organized Beltrami states can only form at very low Reynolds numbers where the kinetic helicity is not even approximately conserved.

At present it remains open whether our observations can be understood in terms of the arguments applicable to turbulence in pipe flow, and further work is currently being carried out. Certainly the value of 4.16 for the upper critical Taylor-Reynolds number must be regarded as tentative in nature. At the same time, our two qualitative arguments both support the idea of the *existence* of such an upper critical Reynolds number. Accordingly, it is of interest to approach the problem from above (as it were) and consider a lower critical Reynolds number for isotropic turbulence to be the asymptotic state of randomly stirred fluid motion. Again, we are not in a position to be precise. Normally, we restrict turbulence runs to $R_\lambda > 40$ (measured in a steady state), but we still have to investigate whether we can establish an actual critical value.

Despite these caveats, the present situation hints at the possibility of a transition region (just as in pipe flow), where the velocity field is neither ordered nor turbulent. Perhaps this is the most surprising aspect of this investigation. Isotropic turbulence, which has been studied intensively for decades on the grounds that it had something in common with shear flows (correlations, spectra), may also have in common that its generation involves a symmetry-breaking phase transition.

M. F. L. thanks Alexander Morozov for helpful discussions about relaminarization of pipe flow. This work has made use of the resources provided by HECToR [12], made available through the Edinburgh Compute and

Data Facility (ECDF) [13]. A. B. is supported by STFC, S. R. Y. and M. F. L. are funded by EPSRC.

-
- [1] T. Kambe, *Geometrical Theory of Dynamical Systems and Fluid Flows*, revised ed. (World Scientific, Singapore, 2010).
 - [2] S. R. Yoffe, *Investigation of the transfer and dissipation of energy in isotropic turbulence*, Ph.D. thesis, University of Edinburgh (2012), <http://arxiv.org/pdf/1306.3408v1.pdf>.
 - [3] W. D. McComb, A. Hunter, and C. Johnston, *Phys. Fluids*, **13**, 2030 (2001).
 - [4] Supplemental Material.
 - [5] S. G. Chumakov, *Phys. Fluids*, **19**, 058104 (2007).
 - [6] S. G. Chumakov, *Phys. Rev. E*, **78**, 15563 (2008).
 - [7] W. D. McComb, *Homogeneous, Isotropic Turbulence: Phenomenology, Renormalization and Statistical Clo-*
sures (Oxford University Press, 2014).
 - [8] T. Mullin and J. Peixinho, in *IUTAM Symposium on Laminar-Turbulent Transition*, edited by R. Govindarajan (Springer, Bangalore, 2006) p. 45.
 - [9] A. P. Willis and R. R. Kerswell, *Phys. Rev. Lett.*, **98**, 014501 (2007).
 - [10] B. Hof, J. Westerweel, T. M. Schneider, and B. Eckhardt, *Nature*, **443**, 59 (2006).
 - [11] B. Eckhardt, T. M. S. B. Hof, and J. Westerweel, *Ann. Rev. Fluid Mech.*, **39**, 447 (2007).
 - [12] Until 2014 HECToR was the UK's national HPC resource. More information can be found at <http://www.hector.ac.uk/>.
 - [13] More information on ECDF can be obtained at <http://www.ecdf.ed.ac.uk/>.

Supplemental Material for “Self-organization and transition to turbulence at low Reynolds numbers in randomly forced isotropic fluid motion”

W. D. McComb,¹ M. F. Linkmann,¹ A. Berera,¹ S. R. Yoffe,² and B. Jankauskas¹

¹*SUPA, School of Physics and Astronomy, University of Edinburgh, UK*

²*SUPA, Department of Physics, University of Strathclyde, Glasgow, UK*

In this Supplemental Material we give further details about our simulations in form of a table of simulation specifications. An additional picture of the visualization is also shown, including an enlarged region.

VISUALIZATION

In order to visualize the Beltrami property of the self-organized state, we plotted vorticity and velocity field vectors in real space in Fig. 1 before and after self-organization. The velocity field is represented by the red arrows and the vorticity field by the blue arrows. The upper image corresponds to of Fig. 3 of the Letter, and the lower image shows more detail by enlargement of selected regions of the upper image. Two observations can be made from the images on the right hand side of Fig. 1, firstly we see alignment between the vorticity and velocity fields, which graphically represents the Beltrami condition and is most clearly visible in the lower image. Secondly, we see only large-scale structure in the flow pattern in the upper image, which is consistent with the measured unimodal energy spectrum shown at long times in Fig. 2 (b) of the Letter. For comparison, the left-hand images in the figure show flow patterns and field vectors before self-organization. The flow pattern is disordered and no alignment between velocity and vorticity can be observed, in fact the fields appear to be mostly orthogonal to each other, reflecting zero kinetic helicity. In terms of spectra, this corresponds to the early-time energy spectra in Fig. 2 (b) of the Letter.

SIMULATION SPECIFICATIONS

N^3	$k_{max}\eta$	$R_{\lambda,SO}$	ν	R_λ	n	t_{max}/s	τ^*	σ/\sqrt{n}
32^3	2.85	12.91	0.1	2.61	99	1000	114.60	10.26
32^3	2.63	15.12	0.09	2.93	99	1000	120.80	5.34
32^3	2.56	15.91	0.087	3.00	100	1000	122.47	4.23
32^3	2.52	16.47	0.085	3.07	100	1000	140.04	6.76
32^3	2.48	17.07	0.083	3.14	100	1000	139.50	5.14
32^3	2.41	18.04	0.08	3.26	100	1000	145.52	5.32
32^3	2.39	18.38	0.079	3.30	100	1000	151.20	5.36
32^3	2.34	19.11	0.077	3.39	100	1000	160.76	6.27
32^3	2.29	19.88	0.075	3.47	100	1000	168.04	6.27
32^3	2.25	20.70	0.073	3.57	100	1000	188.26	6.27
32^3	2.18	22.04	0.07	3.72	99	1000	226.35	12.50
32^3	2.16	22.52	0.069	3.78	99	1000	234.59	10.60
64^3	5.26	15.12	0.09	2.93	1	1000	84.50	-
64^3	4.82	18.04	0.08	3.26	1	1000	185.82	-
64^3	4.36	22.04	0.07	3.72	1	1000	321.88	-

TABLE I. Specifications of simulations. N^3 denotes the number of collocation points, k_{max} the largest resolved wavenumber, η the Kolmogorov microscale, $R_{\lambda,SO}$ the Taylor-Reynolds number in the self-organized state, ν the kinematic viscosity, R_λ the initial Taylor-Reynolds number, n the ensemble size, t_{max} the time the simulations were evolved for, $\tau^* = \langle \tau \rangle$ the average time at which the self-organized state is reached and σ is the standard deviation of τ .

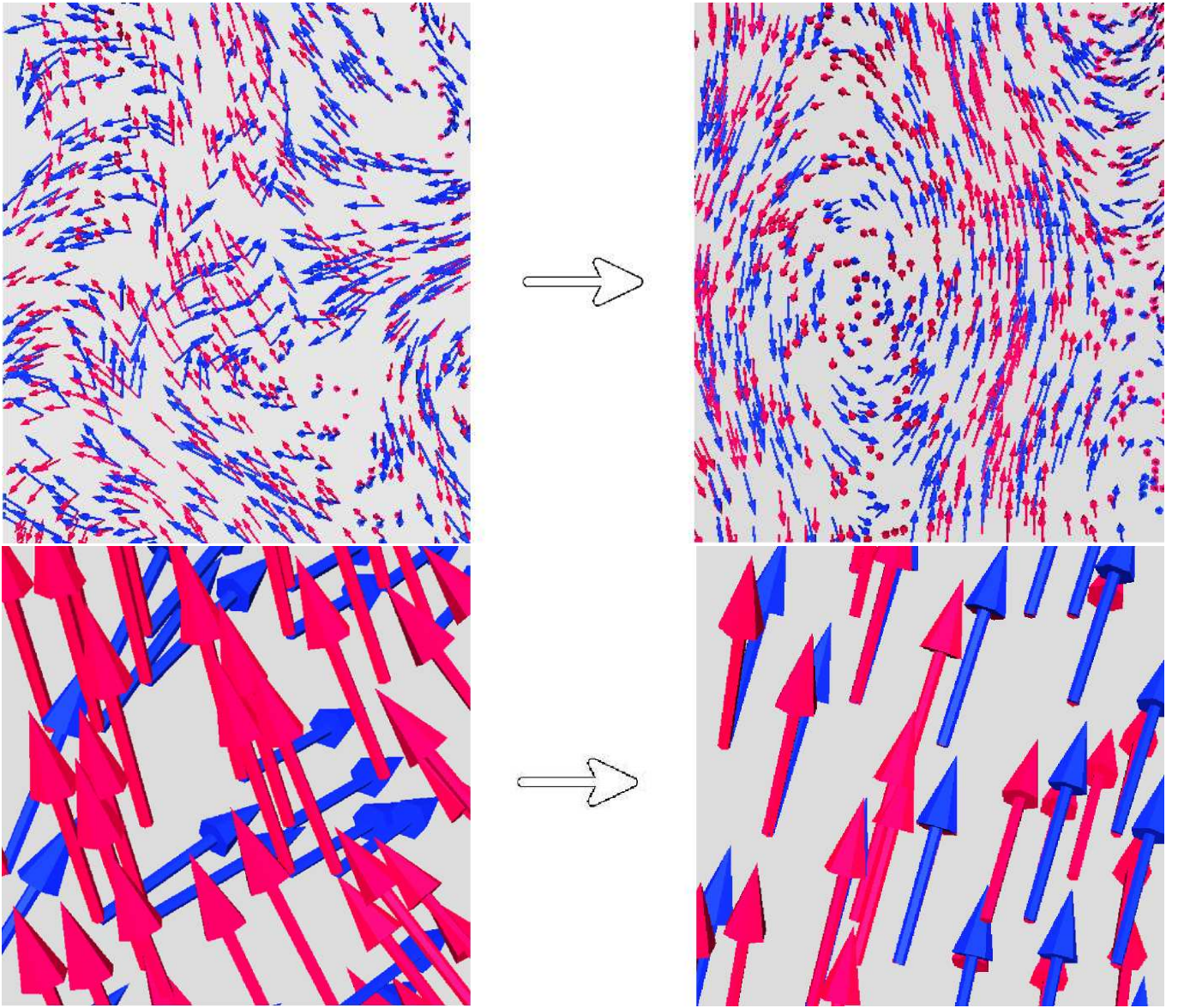


FIG. 1. Visualization of the velocity field (red arrows) and the vorticity field (blue arrows) in x -space before and after self-organization. The lower images show more detail by enlargement of regions in the upper images, while the upper images show the complete simulation box viewed from one side. The alignment between velocity and vorticity fields is clearly visible in the bottom right-hand image, while no such alignment can be seen in the bottom left-hand image. The top right-hand image shows only large-scale flow patterns, unlike the top left-hand image.